Tissue Engineering

DOI: 10.1089/ten.TEA.2017.0044

Title: Role of Bone Marrow Mononuclear Cell Seeding for Nanofiber Vascular Grafts

Authors: Takuma Fukunishi, MD[1, #], Cameron A. Best, BA[2, #], Chin Siang Ong, MD[1], Tyler Groehl, PhD[3], James Reinhardt, PhD[2], Tai Yi, MD[2], Hideki Miyachi, MD, PhD[2], Huaitao Zhang, BS[1], Toshiharu Shinoka, MD, PhD[2], Christopher K. Breuer, MD[2], Jed Johnson, PhD[3], Narutoshi Hibino, MD, PhD[1, *]

Affiliations:

[1] Department of Cardiac Surgery, John Hopkins University, Baltimore, MD

[2] Tissue Engineering and Surgical Research, Nationwide Children's Hospital, Columbus, OH

[3] Nanofiber Solutions, Inc. Columbus, OH

[#] Equally contributing first authors

Manuscript Metrics:

Abstract word count: 287, Main text word count: 4225, References: 35, Figures: 6

Presentation:

15th Biennial Meeting of International Society for Applied Cardiovascular Biology (ISACB), Banff, Alberta, Canada, September 7-10, 2016

[*] **Corresponding Author:**

Narutoshi Hibino, MD, PhD

Department of Cardiac Surgery

Johns Hopkins University

1800 Orleans Street, Zayed 7107, Baltimore, MD, 21287, USA

Tel: +1-410-955-2800

Fax: +1-410-955-3809

E-mail: nhibino1@jhmi.edu

Tissue Engineering
Role of Bone Marrow Mononuclear Cell Seeding for Nanofiber Vascular Grafts (DOI: 10.1089/ten.TEA.2017.0044)
This paper has been peer-reviewed and accepted for publication, but has yet to undergo copyediting and proof correction. The final published version may differ from this proof.

Tissue Engineering
Role of Bone Marrow Mononuclear Cell Seeding for Nanofiber Vascular Grafts (DOI: 10.1089/ten.TEA.2017.0044)
This paper has been peer-reviewed and accepted for publication, but has yet to undergo copyediting and proof correction. The final published version may differ from this proof.

Abstract

Objective: Electrospinning is a promising technology that provides biodegradable nanofiber scaffolds for cardiovascular tissue engineering. However, success with these materials has been limited, and the optimal combination of scaffold parameters for a tissue-engineered vascular graft (TEVG) remains elusive. The purpose of the present study is to evaluate the effect of bone marrow mononuclear cell (BM-MNC) seeding in electrospun scaffolds to support the rational design of optimized TEVGs.

Methods: Nanofiber scaffolds were fabricated from co-electrospinning a solution of polyglycolic acid and a solution of poly(ι-lactide-co-ε-caprolactone) and characterized with scanning electron microscopy. Platelet activation and cell seeding efficiency were assessed by ATP secretion and DNA assays respectively. Cell-free and BM-MNC seeded scaffolds were implanted in C57BL/6 mice (n = 15/group) as infrarenal inferior vena cava (IVC) interposition conduits. Animals were followed with serial ultrasonography for 6 months, after which grafts were harvested for evaluation of patency and neotissue formation by histology and immunohistochemistry (n=10/group) and PCR (n=5/group) analyses.

Results: BM-MNC seeding of electrospun scaffolds prevented stenosis compared to unseeded scaffolds (seeded: 9/10 patent vs. unseeded: 1/10 patent, $p = 0.0003$). Seeded vascular grafts demonstrated concentric laminated smooth muscle cells, a confluent endothelial monolayer, and collagen-rich extracellular matrix. Platelet derived ATP, a marker of platelet activation, was significantly reduced after incubating thrombin-activated platelets in the presence of seeded scaffolds compared to unseeded scaffolds ($p < 0.0001$). In addition, reduced macrophage infiltration and a higher M2 macrophage percentage was observed in seeded grafts.

Conclusions: The beneficial effects of BM-MNC seeding apply to electrospun TEVG scaffolds by attenuating stenosis through the regulation of platelet activation and inflammatory macrophage function, leading to well-organized neotissue formation. BM-MNC seeding is a valuable technique that can be used in the rational design of optimal TEVG scaffolds.

Keywords: Tissue-engineered vascular graft (TEVG), bone marrow mononuclear cell (BM-MNC) seeding, nanofiber, electrospinning, biodegradable scaffold, stenosis

Tissue Engineering
Role of Bone Marrow Mononuclear Cell Seeding for Nanofiber Vascular Grafts (DOI: 10.1089/ten.TEA.2017.0044)
This paper has been peer-reviewed and accepted for publication, but has yet to undergo copyediting and proof correction. The final published version may differ from this proof.

Introduction

Electrospinning has been increasingly explored as a fabrication method to create seamless biodegradable tubular scaffolds for vascular tissue engineering, with applications ranging from surgical reconstruction of congenital cardiac anomalies to small diameter bypass grafting in atherosclerotic coronary artery disease.[1-4] Electrospinning is a rapid, reproducible, and highly customizable technique that can be used to fabricate scaffolds of various geometries.[5] Varying electrospinning process parameters can yield tissue-engineered scaffolds made of dry, nonwoven polymer fibers, ranging in diameter from 50nm to 20μm, smaller than what most other available fiber spinning techniques can produce.[3] The nanoarchitecture of electrospun scaffolds is especially relevant in tissue engineering as it mimics native extracellular matrix (ECM) in scale, which is thought to encourage cellular ingrowth, ECM deposition, and neotissue formation.[6] However, the sequential layering of nanofibers in the construction of tubular TEVG scaffolds produces constructs with three-dimensional pore sizes that are limited by fiber diameter. The effect of small pores (<10μm) in TEVG scaffolds has been recently explored, and most published reports indicate that small pores inhibit cellular infiltration, delay degradation, and support chronic inflammation.[7-11] The latter aspect hinders the immune-mediated process of neovessel formation[7, 12, 13] which in turn may support adverse remodeling such as calcification or chronic intimal hyperplasia. Despite the fact that many innovative electrospun homopolymers, copolymers, and polymer blends have been created in response to these challenges, there is no electrospun scaffold design that has been translated to clinical application.[6]

The first human clinical trial investigating the use of TEVGs in children with congenital heart defects began in 2001.[14] Highly porous biodegradable polymeric scaffolds, comprised of poly(L-lactide-co-ε-caprolactone) (PLCL) reinforced by polyglycolic acid (PGA) mesh[15], were seeded with bone marrow mononuclear cell (BM-MNC). There is now established clinical evidence to show that TEVGs are safe and effective to use in pediatric patients undergoing extracardiac total cavopulmonary connection procedure.[16, 17]

Tissue Engineering
Role of Bone Marrow Mononuclear Cell Seeding for Nanofiber Vascular Grafts (DOI: 10.1089/ten.TEA.2017.0044)
This paper has been peer-reviewed and accepted for publication, but has yet to undergo copyediting and proof correction. The final published version may differ from this proof.

In this report, we fabricated a co-electrospun scaffold from PGA and PLCL modeled after those materials recently reported in human trial.[3, 15-17] Due to reports of BM-MNC seeding preventing TEVG stenosis in other scaffold types,[18] we investigated whether BM-MNC seeding prior to implant improved the performance of electrospun scaffolds in a murine venous interposition model over a 6-month time course.

Materials and Methods

1. Animal care and ethics statement

All animals received humane care in compliance with the National Institutes of Health Guide for the Care and Use of Laboratory Animals. The Institutional Animal Care and Use Committee of the Research Institute at Nationwide Children's Hospital approved and monitored all animal procedures described in this report. Thirty-five C57BL/6 mice (17-20g, 8-12 week old, female) were purchased from Jackson Laboratories (Bar Harbor, ME).

2. Graft fabrication

To create the co-electrospun polyglycolic acid (PGA) and polylactide-co-caprolactone (PLCL) scaffolds, 10 wt% PGA was dissolved in hexafluoroisopropanol and 5 wt% PLCL was dissolved in hexafluoroisopropanol. Each solution was stirred via a magnetic stir bar for at least 3 hours at room temperature. In separate syringes, the PGA solution was dispensed at a flow rate of 2.5 mL/hour and the PLCL solution was dispensed at a flow rate of 5.0 mL/hour to create grafts with a 1:1 PGA:PLCL weight ratio. Both solutions were simultaneously electrospun onto the mandrel that was positioned 20 cm from the needle tips and rotated at 30 RPM. A +25 kV charge was applied to each syringe tip and electrospun nanofibers were deposited onto the grounded mandrel until the desired wall thickness of 0.1mm was achieved. The electrospun scaffold was then removed from the mandrel and the wall thickness measured with a digital snap gauge by placing the scaffold between two glass slides. The PGA/PLCL tubes were cut into 5mm lengths and the inner

diameter was 1mm. The scaffolds were then packaged in Tyvek pouches and sterilized with 25 kGy of gamma irradiation.

3. Scaffold degradation

Electrospun sheets were prepared from the same co-electrospinning setup as used to produce the tubes for this experiment, except the fibers were deposited onto a flat plate to a thickness of approximately 250 μm. The scaffold degradation samples were 250um thick to follow the guidelines outlined in the American Society for Testing and Materials Standard Test Method for Tensile Properties of Plastics (ASTM D638). The difference in thickness does not affect the mechanics of the graft as we report the ultimate tensile strength (UTS) in MPa which is independent of scaffold thickness. The degradation rate is not affected by the scaffold thickness because the construct is completely porous. The thickness of every test sample was measured prior to testing. A digital caliper (VWR) with an accuracy of two decimal places was zeroed on two 3" x 1" x 1 mm glass microscope slides (VWR). Samples were placed between the glass slides, and the thicknesses were measured following ASTM standard D6988-13. Three measurements were taken, one on the right, center, and left of each sample. The median of these three measurements was recorded in millimeters as the thickness of the sample.

Five tensile dogbones were cut from the electrospun sheets according to ASTM D638 Type V using a universal testing machine (MultiTest 5-i, Mecmesin Corporation). For the *in vitro* degradation, a single tensile dogbone was placed in a glass vial with 25 mL of phosphate buffered saline (PBS). Five samples per timepoint were placed in an incubator and held at a constant 37°C until they were withdrawn for mechanical testing. The ends of each dogbone sample were clamped to opposite arms of the testing machine and pulled apart until failure. The peak load from each sample was averaged and recorded in MPa as the ultimate tensile strength (UTS). The elongation to failure of each sample was also recorded as % of original sample length. Young's modulus of each sample was determined from the slope of the linear regime of the resulting stress-strain curve and recorded in MPa.

This paper has been peer-reviewed and accepted for publication, but has yet to undergo copyediting and proof correction. The final published version may differ from this proof.
Tissue Engineering
Role of Bone Marrow Mononuclear Cell Seeding for Nanofiber Vascular Grafts (DOI: 10.1089/ten.TEA.2017.0044)

4. Bone marrow harvest and graft seeding

Clinically, we have already used BM-MNCs as a cell source.[16, 17] As a large number of cells can be obtained from BM-MNCs without further in vitro culture, there are fewer steps in the preparation of tissue engineered vascular grafts. This means a lower risk of contamination, less work and less time needed to fabricate the TEVGs. In addition, these cells have the potential to differentiate into both smooth muscle cells and endothelial cells.[15, 19]

Bone marrow donor mice (n = 5) were administered an overdose cocktail of ketamine (300mg/kg) and xylazine (30mg/kg). Their bone marrow was harvested, the MNC population enriched, and scaffolds seeded as previously described.[18, 20] Briefly, hind limbs were disarticulated in sterile fashion, muscle and tendon dissected, and the femoral and tibial heads were removed. Bone marrow was collected by repeated flushing with 5.0mL of RPMI 1640 (Sigma) + 1% penicillin/streptomycin (P/S, Sigma). The pooled bone marrow was filtered to remove bone spicules and macroaggregates (100µm cell strainer, Fisher). The bone marrow aspirate was layered on Ficoll Histopaque solution (1083, Sigma) in a 1:1 ratio in volume. After density gradient centrifugation the mononuclear cell layer was carefully collected, washed twice with 1x PBS, and resuspended at a concentration of $2.0x10^8$ cells/mL in RPMI-1640 + 1%P/S. Cell concentrations were determined with Trypan blue exclusion using a Countess™ automated cell counter (Invitrogen) as the mean of two separate cell counts. Prior to seeding, grafts were pre-wet by applying 5µL of 1xPBS + 1%P/S to the scaffold lumen for 5:00 min. Excess PBS was aspirated, and 5µL of BM-MNCs ($1.0x10^6$ cells) was introduced to the scaffold lumen. After 10 minutes incubation to allow for cell attachment, a 22G needle was threaded through the lumen before immersion in 1mL of RPMI-1640 + 1%P/S in a 24-well plate. Seeded grafts were incubated overnight at 37°C 5% CO_2 prior to implantation. Efficacy of cell seeding was verified with SEM and PicoGreen dsDNA assay.

5. Graft implantation

Seeded or unseeded scaffolds (n=15/group) were implanted as infrarenal inferior vena cava (IVC) interposition grafts following standard microsurgical technique as previously described.[18, 20, 21] Briefly, mice were administered a pre-anesthesia analgesic of ketoprofen (5mg/kg, IP) and anesthetized with a cocktail of ketamine (100mg/kg, IP) and xylazine (10mg/kg, IP). Scaffolds (5.0 mm length) were interposed end-to-end with 10-0 nylon suture in running fashion. After confirming patent anastomosis and ensuring hemostasis, the abdomen was closed in two layers with 6-0 prolene suture in running fashion. Animals were followed for 6 months without anti-platelet or anti-coagulation therapy. There was no operative and graft related mortality at any point during follow up.

6. Ultrasound interrogation

Implanted grafts were monitored longitudinally until explant (2, 4, 8, 12, and 24 weeks after implantation) with high frequency Doppler ultrasonography (Vevo® 2100, VisualSonics Inc., Toronto, Canada). Anesthesia was induced with 1.5% inhaled isoflurane vaporized with 100% O_2 at a rate of 1L/min. Body temperature was maintained at 38°C and vitals were maintained within normal limits for the duration of ultrasound examination. Long axis images were acquired with B-mode, pulse-wave, and color Doppler. ImageJ (NIH, Bethesda, MD) was used to quantify lumen diameter of B-mode images and graft patency was determined with pulse-wave and color Doppler images as previously described.[12]

7. Graft explant and tissue analysis

After 6-months of follow up, animals were euthanized by administration of an overdose cocktail of ketamine (300 mg/kg) and xylazine (30 mg/kg) followed by induction of pneumothorax. Mice were systemically perfused with cold phosphate buffered saline (1x PBS). Grafts intended for reverse transcription quantitative polymerase chain reaction (RT-qPCR) experiments (n=5/group) were explanted and embedded in OCT compound (optimal cutting temperature, Tissue-Tek, Sakura) on dry ice. Grafts intended for histologic

and immunohistochemical analyses (n=10/group) were perfusion fixed with 10% neutral buffered formalin (Fisher) prior to explant.

7-1. Histology

Formalin fixed samples were dehydrated, paraffin embedded, and serially sectioned (4μm thick). Histologic stains were performed in one batch following standard technique and included hematoxylin and eosin, Masson's Trichrome, von Kossa, Hart's, and Picro Sirius Red. Quantification of lumen diameter was performed with ImageJ by division of luminal circumference by π, and the incidence of stenosis was calculated as the ratio of patent to occluded grafts in each group. A graft was considered patent if the measured lumen diameter was ≥ 75% of the original lumen diameter of the scaffold at implantation.

7-2. Immunohistochemistry and immunofluorescence

For immunohistochemistry, slides were deparaffinized, rehydrated, and blocked for endogenous peroxidase activity (0.3% H_2O_2 in MeOH). Antigens were retrieved via the citrate buffer method (pH 6.0, 90° C for 15min). Slides were blocked for non-specific background staining (Background Sniper, BioCare Medical) before overnight incubation at 4°C with the following primary antibodies: F4/80 (1:1000, Abd Serotec), iNOS (1:200, Abcam), CD206 (1:100, Abcam), αSMA (1:500, Dako), CD31 (1:50, Abcam), and SM-MHC (1:1000, Abcam). For immunohistochemistry, sequential incubation with species-appropriate biotinylated secondary antibodies (1:300-500, Dako) and Horseradish Peroxidase Streptavidin (Dako) identified antibody binding. Chromogenic detection was performed by development with 3,3-diaminobenzidine (Vector). Nuclei were identified via hematoxylin counterstain (Gill's Formula, Vector). Immunofluorescence was performed by incubation with a cocktail of species appropriate Alexa-Fluor®-647 or -488 secondary antibodies (1:300, Life Technologies) followed by nuclear counterstaining with 4'-6 diamidino-2-phenylindole (DAPI, Vector).

7-3. RT-qPCR

Frozen tissue blocks were sliced (30μm thick sections) on a CM1950 cryostat (Leica Biosystems, Buffalo Grove, IL). Sections were washed in 1x PBS to remove excess OCT compound and total RNA was extracted and purified using the RNeasy mini kit (Qiagen). Reverse transcription was performed using the High Capacity RNA-to-cDNA Kit (Applied Biosystems) following the manufacturer's instructions. Quantitative PCR assay was performed with the Step One Plus Real-Time PCR System using the TaqMan Universal PCR Master Mix Kit (Applied Biosystems). Total reaction volume was 20μL: 10μL TaqMan Fast Advanced Master Mix (2x), 1μL Taqman Gene Expression Assay (20x), 7μL nuclease free H_2O, 2μL cDNA. All gene expression assays were obtained from Applied Biosystems (Nitric oxide synthase 3 and smooth muscle alpha 2 actin). All assays were performed in duplicate and values were analyzed using the comparative threshold cycle method and normalized to the expression of the endogenous reference genes HPRT or GAPDH. Gene expression in seeded samples is reported as a relative value (ΔΔCT) to that of unseeded samples (n=5/group).

8. Scanning electron microscopy

For characterization of pore size and fiber diameter, a total of 10 scaffolds were cut open. After dehydration with hexamethyldisilazane, samples were prepared by gold sputter coating and 10 images of the luminal surface were obtained by scanning electron microscopy (SEM) with a Hitachi S-4800 Scanning Electron Microscope at 5.0 – 15.0 kV, for each scaffold. Pore size, which is the area surrounded by 3 or 4 nanofiber, and fiber diameter were determined by acquisition of 30 measurements with perimeters and diameter per SEM image using ImageJ (NIH).

Tissue Engineering
Role of Bone Marrow Mononuclear Cell Seeding for Nanofiber Vascular Grafts (DOI: 10.1089/ten.TEA.2017.0044)
This paper has been peer-reviewed and accepted for publication, but has yet to undergo copyediting and proof correction. The final published version may differ from this proof.

9. In vitro analyses

9-1. DNA assay

The fluorometric Quant-iT™ PicoGreen® dsDNA Assay Kit (Life Technologies) was used following the manufacturer's protocol to monitor cell seeding (n=5, seeded scaffolds). Fluorescence intensity measurements were acquired with a SpectraMax M5 Microplate reader (Excitation 488nm, Emission 525nm, Molecular Devices) and applied to a standard curve. The efficacy of cell seeding was determined by the total number of cells in each well divided by the surface area of the scaffold (cells/ mm^2) as previously described.[18]

9-2. Platelet isolation and ATP secretion assays

Whole blood was harvested by cardiac puncture using a 25G needle and 3mL syringe pre-loaded with 100-200µL of citrate-dextrose solution (C3821, Sigma) and platelets were enriched as previously described.[22] Briefly, aspirated blood was centrifuged (120g, 8min) to separate erythrocytes and leukocytes from the platelet rich plasma (PRP). PRP was aspirated and centrifuged (120g, 3min) to further enrich the platelet fraction. The supernatant was centrifuged (740g, 10min) to yield a pellet that was then re-suspended with 200µL of 1x PBS. Platelet concentration was quantified using an ABX Micros 60 hematology analyzer (Horiba) and determined as the mean of two separate measurements. Cells were resuspended in 1x PBS at a concentration of $1x10^4$ cells/µL. 50µL of platelet suspension ($5.0x10^5$ platelets) were added to the wells of a black polystyrene 96-well microplate (Corning Costar) containing either BM-MNC seeded (n=18) or unseeded (n=10) scaffolds under either thrombin-activated (0.1U/mL) or resting conditions. Plates were incubated at room temperature with gentle shaking for 1.0 hr, after which grafts were removed from the wells. The concentration of platelet-derived ATP in each well was determined by addition of 50µL ChronoLume™ reagent (Chrono-Log Corp.) followed by luminescent detection with a LUMIstar Omega microplate luminometer (BMG Labtech) as previously described.[23] Measured values were applied to a standard curve and the degree of platelet ATP secretion in each condition was determined.

Tissue Engineering
Role of Bone Marrow Mononuclear Cell Seeding for Nanofiber Vascular Grafts (DOI: 10.1089/ten.TEA.2017.0044)
This paper has been peer-reviewed and accepted for publication, but has yet to undergo copyediting and proof correction. The final published version may differ from this proof.

10. Statistical Analysis

Lumen diameter measurements derived from serial ultrasound imaging were analyzed via two-way ANOVA with Tukey's correction for multiple comparisons. Histomorphometric quantifications of lumen diameter were compared with nonparametric unpaired two-tailed Mann Whitney t-test, as the data were not normally distributed. The incidence of stenosis between both groups was compared with a two-sided Chi-square test. $F4/80^+$ cell counts and SEM measurements of fiber diameter and pore size were analyzed with a parametric unpaired two-tailed t-test. iNOS and CD206 IHC and PCR, eNOS and ACTA2 PCR, and ATP secretion data were compared within and across groups by two-way ANOVA with Tukey's correction for multiple comparisons. $p < 0.05$ was considered statistically significant.

Results

1. PGA/PLCL scaffolds comprised of nanofibers forming pores of < 10μm

The mean fiber diameter and pore size of the PGA/PLCL electrospun scaffold for lumen surface was 0.61 ± 0.27μm and 9.71 ± 0.16μm, respectively. SEM images of scaffold are shown in Figure 1A-C. The results of mechanical testing of *in vitro* degraded PGA/PLCL scaffolds are shown in Figure 1G-I. The average ultimate tensile strength (UTS) of the scaffolds decreased from 7.47 ± 0.83 MPa to 1.96 ± 0.89 MPa in two weeks. After 12 weeks, the scaffolds' average UTS decreased to 0.11 ± 0.09 MPa. No material remained viable for testing at longer time periods. After four weeks, the scaffold's Young's Modulus decreased from 29.06 ± 11.65 MPa to 1.44 ± 0.66 MPa. The elongation to failure decreased to 324 ± 39% after 1 week, increased to 832 ± 20% after 4 weeks, and then finally decreased to 46 ± 8% at 12 weeks (Fig .1G, H, I).

2. BM-MNC seeding of PGA/PLCL nanofiber scaffolds prevents acute graft narrowing and chronic stenosis

Serial ultrasound of TEVG implants performed at 2, 4, 8, 12, and 24 weeks after graft implantation indicated a significant difference in lumen diameter between the seeded and unseeded groups as early as 4 weeks after implantation ($p < 0.001$, Fig. 2A). This difference was maintained throughout the duration of follow up. Histomorphometric analysis after explant confirmed that the lumen diameter and graft patency of seeded grafts was significantly greater than those of unseeded grafts (Lumen diameter: 1074 ± 295.8 µm in seeded vs. 252.3 ± 281.2 µm in unseeded ; $p < 0.0001$, Fig. 3A; Graft patency: 90% in seeded vs. 10% in unseeded : $p = 0.0003$, Fig. 3B).

3. BM-MNC seeded PGA/PLCL scaffolds demonstrate vascular neotissue formation and extracellular matrix deposition after 6 months

Histologic comparison between seeded and unseeded scaffolds demonstrated vascular neotissue formation in seeded grafts characterized by mature ECM on the luminal and adventitial graft surfaces (Masson's Trichrome and Picrosirius Red, Fig. 3 E, H) and appreciable cellular infiltration (H&E, Fig.3 E). In unseeded grafts, stenotic tissue was characterized by excessive ECM deposition (Fig. 3 I, L). Little to no elastin deposition occurred in either group (Hart's, Fig. 3 G, K). Minimal vascular calcification was observed, despite the limited *in vivo* degradation of the scaffold (Fig. 3 F, J).

4. BM-MNC seeding modulates host inflammation

Immunohistochemical staining for $F4/80^+$ macrophages demonstrated significantly less macrophage infiltration in seeded scaffolds at 6 months (Fig. 4 A, B, G, $p < 0.05$). Regarding macrophage phenotype (Fig. 4C-F), there was a trend that the number of iNOS positive cells in seeded scaffolds was smaller than that in unseeded scaffolds, which did not reach statistical difference (Fig. 4H, $p = 0.14$). The number of CD206 positive cells was significantly higher in seeded scaffolds (Fig. 4H, $p < 0.0001$).

5. Cell-seeded nanofiber scaffolds support formation of well-organized luminal neotissue

Immunofluorescent analysis of TEVG neotissue indicated the formation of well-organized neo-intima in the seeded group characterized by a medial α-SMA$^+$ smooth muscle cell layer lined by a CD31$^+$ endothelial cell monolayer (Fig. 5 A-B). Subsequent staining for SM-MHC in the seeded group confirmed that the luminal smooth muscle cells were mature and contractile (Fig. 5 B inset). As expected, the unseeded TEVG neotissue was characterized by an unorganized population of α-SMA$^+$ and CD-31$^+$ cells (Fig. 5 C), and evidence of re-canalization was appreciated (Fig. 5 D). RT-qPCR indicated less ACTA2 gene transcription and significantly more eNOS transcription in the seeded group (Fig. 5 E, $p < 0.005$).

6. BM-MNC seeding of electrospun PGA/PLCL scaffolds attenuated platelet derived ATP

Since the occlusive luminal narrowing of the unseeded TEVGs was observed as early as 4 weeks after implantation, we suspected thrombosis and therefore investigated the interaction of activated platelets (distinguished by increased ATP secretion) with seeded and unseeded scaffolds *in vitro.* Platelets are among the first immune cells to interact with an implanted vascular graft, and aberrant platelet activation could initiate a cascade involving thrombus formation, fibrin deposition, inflammatory cell recruitment, mesenchymal cell proliferation, and progressive neo-intimal hyperplasia. We found a significant difference in the quantity of measureable ATP from thrombin-activated platelets between seeded and unseeded scaffolds ($p < 0.001$). Interestingly, while a significant difference in the amount of ATP secreted between thrombin-activated and resting platelets in the unseeded group ($p < 0.001$) was found, no difference was appreciated in the seeded group, suggesting that BM-MNC seeding may attenuate adverse platelet function.

This paper has been peer-reviewed and accepted for publication, but has yet to undergo copyediting and proof correction. The final published version may differ from this proof.
Tissue Engineering
Role of Bone Marrow Mononuclear Cell Seeding for Nanofiber Vascular Grafts (DOI: 10.1089/ten.TEA.2017.0044)

Discussion

The results of this study demonstrated the effect of BM-MNC seeding in a novel electrospun vascular graft. BM-MNC seeding of nanofiber scaffolds prevented stenosis, compared to unseeded scaffolds over 6 months. The patent vascular grafts showed concentric laminated smooth muscle cells, a confluent endothelial monolayer, and collagen rich ECM. Platelet derived ATP was significantly reduced after incubating thrombin-activated platelets in the presence of BM-MNC seeded nanofiber scaffolds compared to unseeded scaffolds. Macrophage infiltration into the cell-seeded grafts was significantly less than unseeded grafts. These data suggest that BM-MNC seeding on nanofiber vascular grafts attenuated stenosis through the prevention of host macrophage infiltration and platelet function, which led to well-organized neotissue formation.

Cell seeding reduces monocyte/macrophage infiltration, expression of proinflammatory markers, and promotes TEVG patency and longevity.[7, 12, 18] We have previously demonstrated that BM-MNC cell seeding effectively attenuates intimal hyperplasia in both murine[7, 12, 18] and ovine[24, 25] models, and that this effect is dose-responsive.[18] However, the scaffolds used in previous reports consisted of a non-woven PGA felt sealed with a polymer solution of PLCL[26] which yielded a microarchitecture permitting a relatively high degree of cell infiltration (pore size: $45.54 \pm 17.6\mu m$), rapid degradation kinetics (loss of tensile strength by 8 weeks), with favorable growth and remodeling over the time course of implantation.[27, 28] The model scaffold examined in this report had a much smaller fiber diameter ($0.61 \pm 0.24\mu m$) and pore size ($9.12 \pm 3.15\mu m$) than previous studies, which represents many electrospun constructs examined in recent literature.[3] Despite much smaller pore size of the scaffold, the role of cell seeding to attenuate inflammation and prevent graft stenosis was similar. These data indicate that the beneficial effects of BM-MNC seeding may, at least to a certain degree, be independent of scaffold type.

Macrophage phenotype (M1/M2) plays an important role in remodeling. Recent studies have suggested that cell-free nanofiber scaffolds directed macrophages into the M1 phenotype.[29, 30] In our previous scaffolds, we have demonstrated that BM-MNCs

seeded into TEVGs reduced the overall influx of macrophages and the magnitude of M1 activation. Moreover, macrophages that infiltrate cell-seeded grafts do not undergo M1 to M2 transition, as was observed in unseeded grafts.[12] It is noted by F4/80 staining, that macrophage infiltration was present in both seeded and unseeded grafts at 6 months due to remaining nanofiber scaffolds, however, this was significantly less in the seeded grafts. Interestingly, by iNOS and CD206 staining, there was higher M2 macrophage infiltration and lower M1 macrophage infiltration noted in the seeded scaffolds compared to the unseeded scaffolds. Daley et al. reported wound-healing macrophages with features of both M1 and M2 activation.[31] Therefore, macrophages that populate cell-seeded grafts assume a unique activation state promoting remodeling, that is yet to be defined. If we can find specific markers of macrophage subtypes that affect graft patency, these would be useful for predicting graft stenosis in the clinical setting.

More recently, the regulation of platelet activity by seeded BM-MNCs has been considered, and significant platelet activation, aggregation, and mural thrombus formation/fibrin deposition is thought to initiate an inflammatory cascade leading to progressive vessel occlusion,[32, 33] which may be the root cause of stenosis observed in our model. In 2007, Hashi et al. revealed the antithrombogenic property of bone marrow mesenchymal stem cells (MSCs) in nanofiber vascular grafts; cross-sectional staining showed platelet activation/aggregation and thrombus formation on the luminal surface of acellular grafts but not of MSC-seeded grafts.[34] In this report, we demonstrated that BM-MNC seeding of our electrospun grafts potently reduced measurable platelet-derived ATP *in vitro*, a molecule co-secreted with ATP from activated platelets that is implicated in the aggregation of platelets to a growing thrombus *in vivo*.

Regarding seeding technique, the traditional cell seeding approach for vascular grafts is known as static cell seeding, and involves the manual pipetting of cells directly onto a graft. However, this technique is operator dependent, as we are using small lumen diameter grafts (1mm) in a murine **infrarenal** IVC interposition model. An operator independent seeding method such as vacuum seeding would be effective for standardization in the future[35].

Tissue Engineering
Role of Bone Marrow Mononuclear Cell Seeding for Nanofiber Vascular Grafts (DOI: 10.1089/ten.TEA.2017.0044)
This paper has been peer-reviewed and accepted for publication, but has yet to undergo copyediting and proof correction. The final published version may differ from this proof.

BM-MNC seeding for nanofiber vascular graft led to the attenuation of inflammation and prevention of graft stenosis, as demonstrated by high M2 and low M1 macrophages infiltration and reduction of measurable platelet-derived ATP *in vitro*.

While the results of this study are promising and clearly encourage further investigation, this experiment was limited by the small animal model and seeding technique in this study. We utilized a murine model for vascular graft implantation, however the typical lifespan of mice is up to 1 to 1.5 years. It is difficult to perform long-term experiments in mice with nanofiber scaffolds.

Conclusion

BM-MNC seeding of electrospun TEVG scaffolds prevents stenosis by modulating host macrophage and platelet function. To our knowledge, we are the first to report the prevention of platelet activation using BM-MNC seeded nanofiber biodegradable scaffolds. Incorporating BM-MNC seeding into novel electrospinning approaches for cardiovascular tissue engineering may improve patency in the venous circulation and allow for the rational design of an optimized electrospun TEVG.

Acknowledgements

The Morphology Core at Nationwide Children's Hospital performed the paraffin embedding, sectioning, and all histologic stains including: H&E, Masson's Trichrome, von Kossa, Hart's, and Picrosirius red. This study was supported by grants from the NIH Center for Accelerated Innovations: Technology Development Program (1UH54HL119810-01) (Dr. Hibino), Thrasher Research Fund Early Career Awards (Dr. Hibino), and by electrospun nanofiber Tissue-Engineered Vascular Grafts from Nanofiber Solutions, Inc.

Tissue Engineering
Role of Bone Marrow Mononuclear Cell Seeding for Nanofiber Vascular Grafts (DOI: 10.1089/ten.TEA.2017.0044)
This paper has been peer-reviewed and accepted for publication, but has yet to undergo copyediting and proof correction. The final published version may differ from this proof.

Author Disclosure Statement

Drs. Breuer and Shinoka receive research support from Gunze Ltd. (Kyoto, Japan) and Cook Regentec (Indianapolis, IN). Dr. Breuer is on the Scientific Advisory Board of Cook Medical (Bloomington, IN). Dr. Hibino receives research support from Secant Medical (Telford, PA). Jed Johnson is a co-founder of Nanofiber Solutions, Inc (Columbus, OH). The remaining authors have no conflicts of interest to disclose.

References:

1. Pham QP, Sharma U, Mikos AG. Electrospinning of polymeric nanofibers for tissue engineering applications: a review. *Tissue Eng.* 2006;12:1197-1211.

2. Cleary MA, Geiger E, Grady C, Best C, Naito Y, Breuer C. Vascular tissue engineering: the next generation. *Trends Mol Med.* 2012;18:394-404.

3. Rocco KA, Maxfield MW, Best CA, Dean EW, Breuer CK. In vivo applications of electrospun tissue-engineered vascular grafts: a review. *Tissue Eng Part B Rev.* 2014;20:628-640.

4. Tara S, Rocco KA, Hibino N, et al. Vessel bioengineering. *Circ J.* 2014;78:12-19.

5. Rathore A, Cleary M, Naito Y, Rocco K, Breuer C. Development of tissue engineered vascular grafts and application of nanomedicine. *Wiley Interdiscip Rev Nanomed Nanobiotechnol.* 2012;4:257-272.

6. Barnes CP, Sell SA, Boland ED, Simpson DG, Bowlin GL. Nanofiber technology: designing the next generation of tissue engineering scaffolds. *Adv Drug Deliv Rev.* 2007;59:1413-1433.

7. Roh JD, Sawh-Martinez R, Brennan MP, et al. Tissue-engineered vascular grafts transform into mature blood vessels via an inflammation-mediated process of vascular remodeling. *Proc Natl Acad Sci U S A.* 2010;107:4669-4674.

8. Tara S, Kurobe H, Rocco KA, et al. Well-organized neointima of large-pore poly(L-lactic acid) vascular graft coated with poly(L-lactic-co-epsilon-caprolactone) prevents calcific deposition compared to small-pore electrospun poly(L-lactic acid) graft in a mouse aortic implantation model. *Atherosclerosis.* 2014;237:684-691.

9. Khosravi R, Best CA, Allen RA, et al. Long-Term Functional Efficacy of a Novel Electrospun Poly(Glycerol Sebacate)-Based Arterial Graft in Mice. *Ann Biomed Eng.* 2016;44:2402-2416.

10. Sugiura T, Tara S, Nakayama H, et al. Fast-degrading bioresorbable arterial vascular

graft with high cellular infiltration inhibits calcification of the graft. *J Vasc Surg.* 2016.

11. Gao Y, Yi T, Shinoka T, et al. Pilot Mouse Study of 1 mm Inner Diameter (ID) Vascular Graft Using Electrospun Poly(ester urea) Nanofibers. *Adv Healthc Mater.* 2016;5:2427-2436.

12. Hibino N, Yi T, Duncan DR, et al. A critical role for macrophages in neovessel formation and the development of stenosis in tissue-engineered vascular grafts. *FASEB J.* 2011;25:4253-4263.

13. Hibino N, Mejias D, Pietris N, et al. The innate immune system contributes to tissue-engineered vascular graft performance. *FASEB J.* 2015;29:2431-2438.

14. Shin'oka T, Imai Y, Ikada Y. Transplantation of a tissue-engineered pulmonary artery. *N Engl J Med.* 2001;344:532-533.

15. Matsumura G, Hibino N, Ikada Y, Kurosawa H, Shin'oka T. Successful application of tissue engineered vascular autografts: clinical experience. *Biomaterials.* 2003;24:2303-2308.

16. Shin'oka T, Matsumura G, Hibino N, et al. Midterm clinical result of tissue-engineered vascular autografts seeded with autologous bone marrow cells. *J Thorac Cardiovasc Surg.* 2005;129:1330-1338.

17. Hibino N, McGillicuddy E, Matsumura G, et al. Late-term results of tissue-engineered vascular grafts in humans. *J Thorac Cardiovasc Surg.* 2010;139:431-436, 436 e431-432.

18. Lee YU, Mahler N, Best CA, et al. Rational design of an improved tissue-engineered vascular graft: determining the optimal cell dose and incubation time. *Regen Med.* 2016;11:159-167.

19. Kurobe H, Maxfield MW, Breuer CK, Shinoka T. Concise review: tissue-engineered vascular grafts for cardiac surgery: past, present, and future. *Stem Cells Transl Med.* 2012;1:566-571.

20. Lee YU, Yi T, Tara S, et al. Implantation of inferior vena cava interposition graft in mouse model. *J Vis Exp.* 2014.

21. Goyal A, Wang Y, Su H, et al. Development of a model system for preliminary evaluation of tissue-engineered vascular conduits. *J Pediatr Surg.* 2006;41:787-791.

22. Tara S, Kurobe H, de Dios Ruiz Rosado J, et al. Cilostazol, Not Aspirin, Prevents Stenosis of Bioresorbable Vascular Grafts in a Venous Model. *Arterioscler Thromb Vasc Biol.* 2015;35:2003-2010.

23. Sun B, Tandon NN, Yamamoto N, Yoshitake M, Kambayashi J. Luminometric assay of platelet activation in 96-well microplate. *Biotechniques.* 2001;31:1174, 1176, 1178 passim.

24. Brennan MP, Dardik A, Hibino N, et al. Tissue-engineered vascular grafts demonstrate evidence of growth and development when implanted in a juvenile animal model. *Ann Surg.* 2008;248:370-377.

25. Kurobe H, Tara S, Maxfield MW, et al. Comparison of the biological equivalence of two methods for isolating bone marrow mononuclear cells for fabricating tissue-engineered vascular grafts. *Tissue Eng Part C Methods.* 2015;21:597-604.

26. Roh JD, Nelson GN, Brennan MP, et al. Small-diameter biodegradable scaffolds for functional vascular tissue engineering in the mouse model. *Biomaterials.* 2008;29:1454-1463.

27. Naito Y, Williams-Fritze M, Duncan DR, et al. Characterization of the natural history of extracellular matrix production in tissue-engineered vascular grafts during neovessel formation. *Cells Tissues Organs.* 2012;195:60-72.

28. Khosravi R, Miller KS, Best CA, et al. Biomechanical diversity despite mechanobiological stability in tissue engineered vascular grafts two years post-implantation. *Tissue Eng Part A.* 2015;21:1529-1538.

29. Wang Z, Cui Y, Wang J, et al. The effect of thick fibers and large pores of electrospun poly(epsilon-caprolactone) vascular grafts on macrophage polarization and arterial

regeneration. *Biomaterials.* 2014;35:5700-5710.

30. Garg K, Pullen NA, Oskeritzian CA, Ryan JJ, Bowlin GL. Macrophage functional polarization (M1/M2) in response to varying fiber and pore dimensions of electrospun scaffolds. *Biomaterials.* 2013;34:4439-4451.

31. Daley JM, Brancato SK, Thomay AA, Reichner JS, Albina JE. The phenotype of murine wound macrophages. *J Leukoc Biol.* 2010;87:59-67.

32. Diaz JA, Obi AT, Myers DD, Jr., et al. Critical review of mouse models of venous thrombosis. *Arterioscler Thromb Vasc Biol.* 2012;32:556-562.

33. Rabinovich A, Cohen JM, Cushman M, Kahn SR, Bio SOXI. Association between inflammation biomarkers, anatomic extent of deep venous thrombosis, and venous symptoms after deep venous thrombosis. *J Vasc Surg Venous Lymphat Disord.* 2015;3:347-353 e341.

34. Hashi CK, Zhu Y, Yang GY, et al. Antithrombogenic property of bone marrow mesenchymal stem cells in nanofibrous vascular grafts. *Proc Natl Acad Sci U S A.* 2007;104:11915-11920.

35. Soletti L, Nieponice A, Guan J, Stankus JJ, Wagner WR, Vorp DA. A seeding device for tissue engineered tubular structures. *Biomaterials.* 2006;27:4863-4870.

Figure Legends

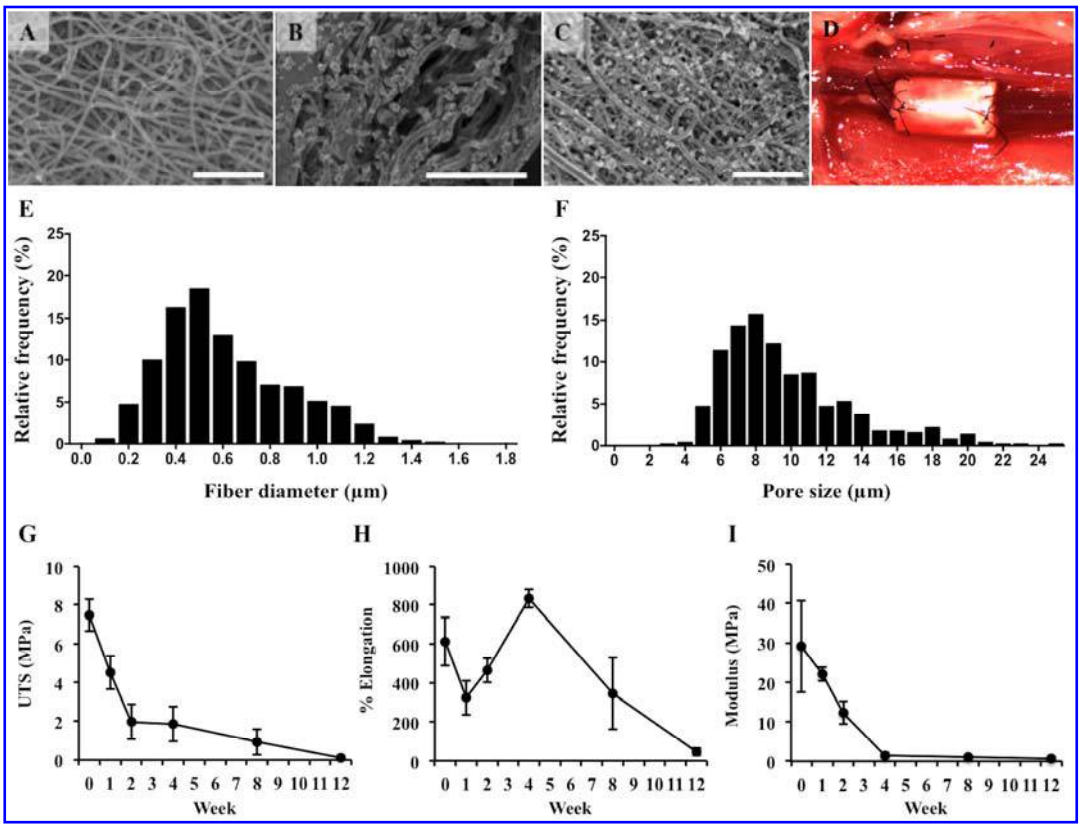

Figure 1. Scaffold characterization. SEM images of luminal (A) and adventitial (B) surfaces of the electrospun scaffold. SEM of a BM-MNC-seeded scaffold luminal surface (C). Implantation of a seeded graft (D) in the murine infrarenal IVC interposition model. Fiber diameter (E) and pore size (F) for luminal surface (Fiber diameter: 0.61 ± 0.27µm, pore size: 9.71 ± 0.16µm). I*n vitro* degradation mechanical values of ultimate tensile strength (UTS) (G), percent elongation to failure (H), and Young's Modulus (I). Scale bar = 50µm.

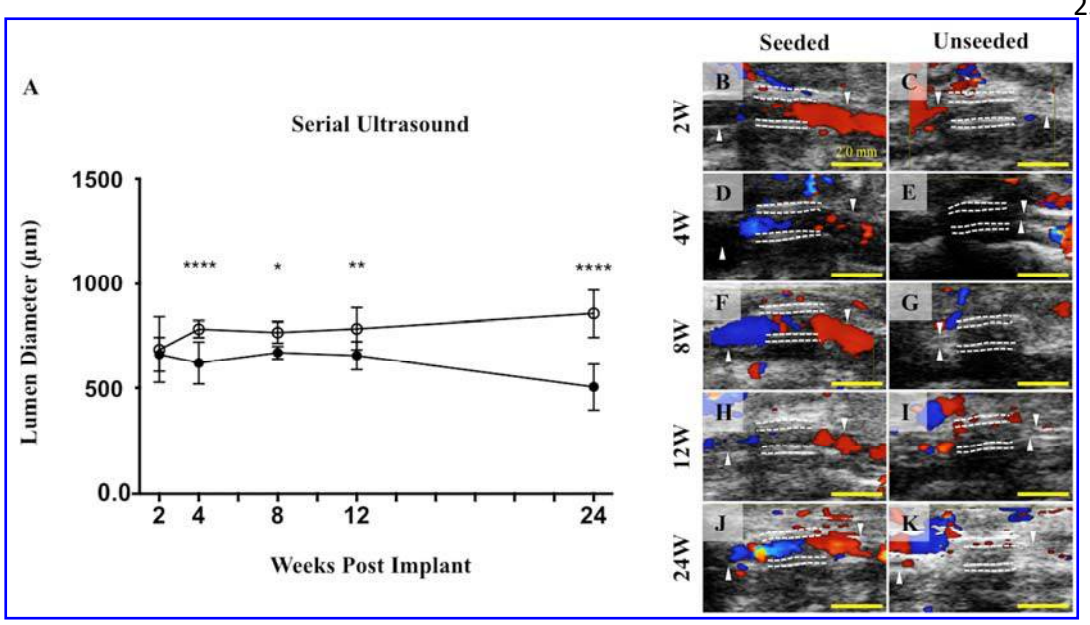

Figure 2. Lumen diameter over time by serial ultrasound. Serial ultrasound of implanted TEVGs performed at 2, 4, 8, 12, and 24 weeks after graft implantation indicated a significant difference in lumen diameter between the seeded and unseeded groups as early as 4 weeks after implantation that was maintained throughout the 6-month time course (A, $^{****}p < 0.0001$, $^{*}p < 0.05$, $^{**}p < 0.005$). Representative ultrasound images from each time points (B-K, respectively), demonstrating patent grafts characterized by color Doppler flow through the lumen (B, D, F, H, J) in the seeded group and occluded grafts in the unseeded group (C, E, G, I, K). Color Doppler signals in the unseeded group may indicate the presence of collateral vasculature surrounding stenotic TEVGs. The white dotted lines indicate the luminal and adventitial surfaces of the TEVGs. Scale bar = 2.0 mm.

Tissue Engineering
Role of Bone Marrow Mononuclear Cell Seeding for Nanofiber Vascular Grafts (DOI: 10.1089/ten.TEA.2017.0044)
This paper has been peer-reviewed and accepted for publication, but has yet to undergo copyediting and proof correction. The final published version may differ from this proof.

Tissue Engineering
Role of Bone Marrow Mononuclear Cell Seeding for Nanofiber Vascular Grafts (DOI: 10.1089/ten.TEA.2017.0044)
This paper has been peer-reviewed and accepted for publication, but has yet to undergo copyediting and proof correction. The final published version may differ from this proof.

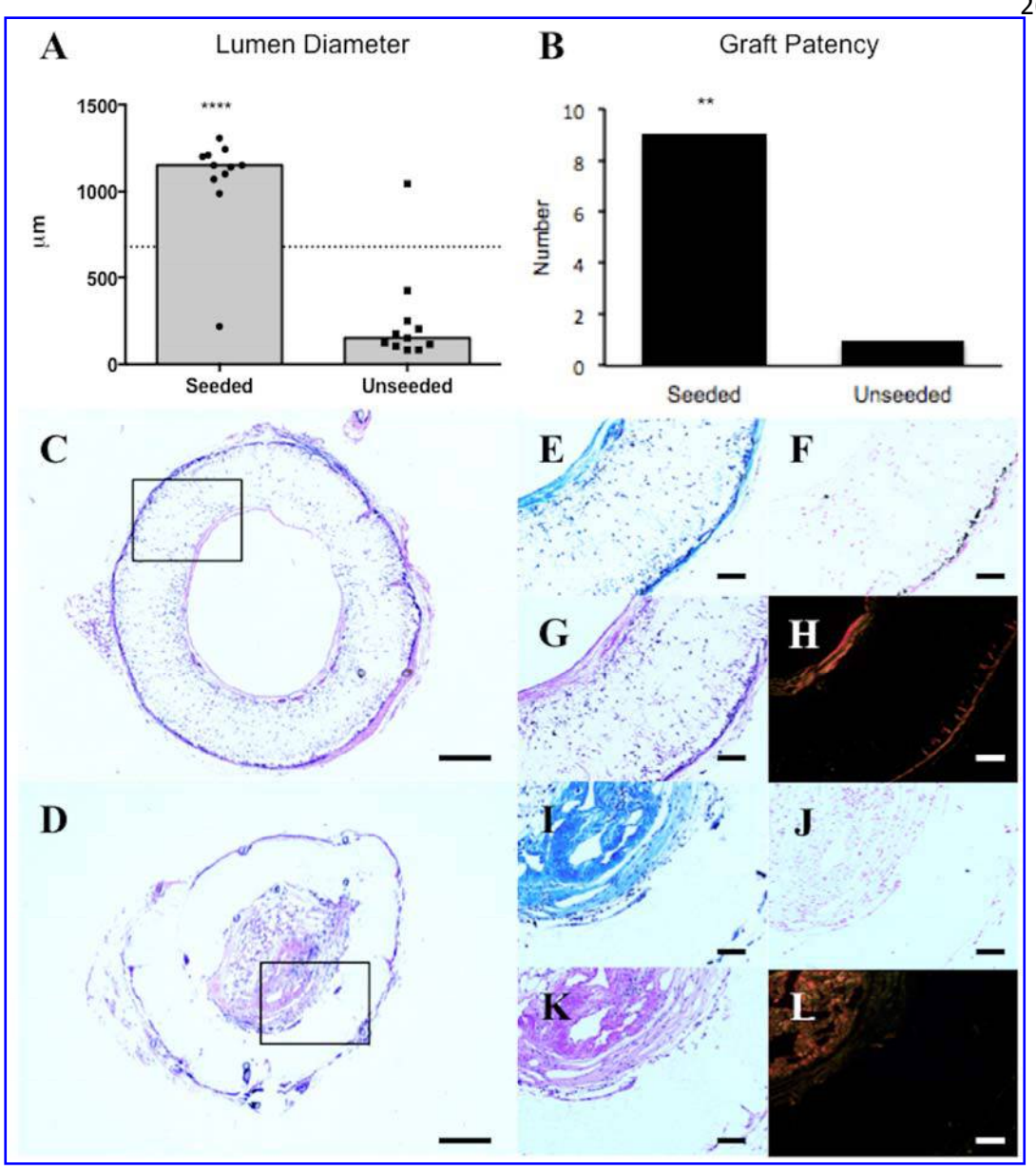

Figure 3. Histological assessment of vascular neotissue formation after 6 months. Histomorphometric comparison of the lumen diameter measurements (A) and graft patency (B) between the seeded and unseeded groups demonstrates that BM-MNC seeding prevents occlusion in the nanofiber scaffold ($^{****}p < 0.0001$, $^{***}p = 0.0003$). Histologic comparison between seeded and unseeded scaffolds demonstrated vascular neotissue formation in seeded grafts characterized by mature extracellular matrix (ECM) on the luminal and adventitial graft surfaces, adequate cellular infiltration, and minimal

vascular calcification. Representative photomicrographs for each group (Seeded: C, E-H; Unseeded: D, I-L) are shown for H&E (C and D), Masson's trichrome (E and I), Hart's (G and K), von Kossa (F and J), and Picrosirius red stains (H and L). Scale bar = 200μm for C and D, and 100μm otherwise.

Tissue Engineering
Role of Bone Marrow Mononuclear Cell Seeding for Nanofiber Vascular Grafts (DOI: 10.1089/ten.TEA.2017.0044)
This paper has been peer-reviewed and accepted for publication, but has yet to undergo copyediting and proof correction. The final published version may differ from this proof.

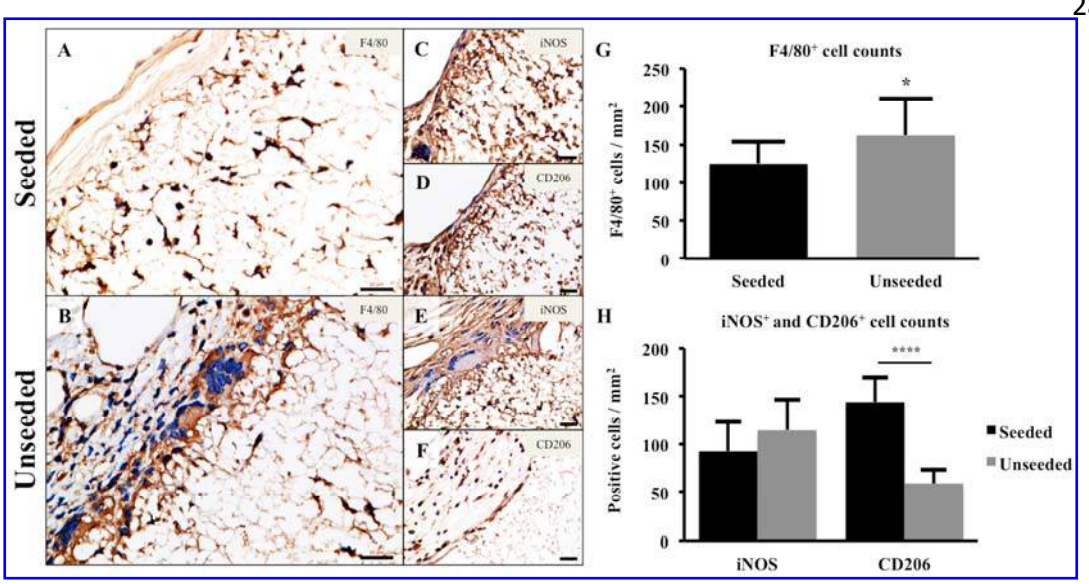

Figure 4. BM-MNC seeding of electrospun TEVG modulated host inflammatory cell infiltration and phenotype. F4/80 staining of seeded (A) and unseeded (B) electrospun TEVGs. Phenotypic characterization of TEVG macrophages demonstrated iNOS$^+$ (Seeded: C; Unseeded: E) and CD206$^+$ (Seeded: D; Unseeded: F) cells. F4/80$^+$ cells in the seeded vs. unseeded group at 6 months (G); seeded group revealed significantly less macrophage infiltration ($^*p < 0.05$). iNOS$^+$ and CD206$^+$ cells in the seeded vs. unseeded group at 6 months (H); unseeded group showed significantly less CD206$^+$ cells ($^{****}p < 0.0001$). Scale bar = 20µm.

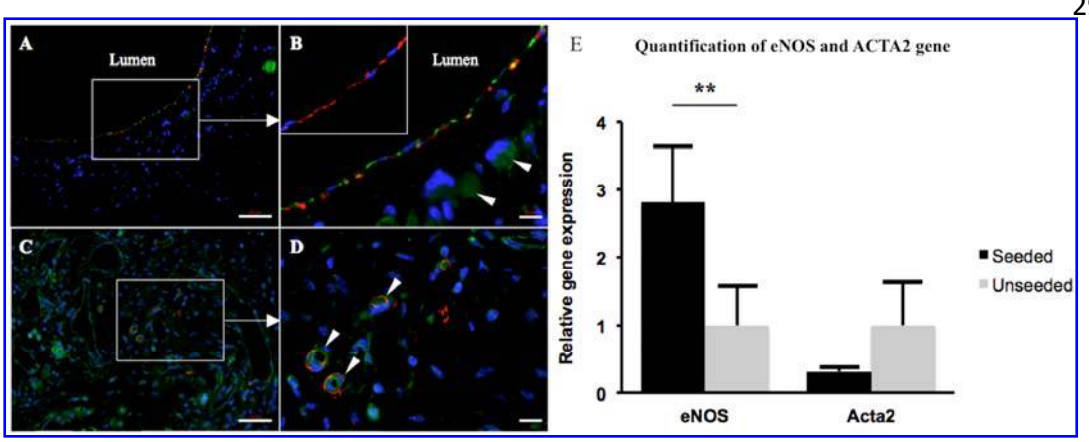

Figure 5. Cell-seeded nanofiber scaffolds are characterized by well-organized and mature vascular neotissue. Immunofluorescent staining of BM-MNC seeded scaffolds indicated the formation of well-organized neo-intima characterized by a medial α-SMA^{+} (red) smooth muscle cell layer lined by CD31^{+} (green) endothelial cells (A, B, arrowheads denote background staining due to remaining scaffold material). SM-MHC staining (red) confirmed that the medial smooth muscle cells in the seeded group were mature and contractile (B, inset). Unseeded TEVG neotissue was characterized by an unorganized population of α-SMA^{+} and CD-31^{+} cells (C), with evidence of re-canalization (D, arrowheads indicate neovascularization of stenotic tissue). Quantification of eNOS and ACTA2 gene transcription by RT-qPCR (E); less ACTA2 and significantly more eNOS gene transcription in the seeded group ($^{**}p < 0.005$). Scale bar = 50µm for A and C, 10µm for B and D.

Tissue Engineering
Role of Bone Marrow Mononuclear Cell Seeding for Nanofiber Vascular Grafts (DOI: 10.1089/ten.TEA.2017.0044)
This paper has been peer-reviewed and accepted for publication, but has yet to undergo copyediting and proof correction. The final published version may differ from this proof.

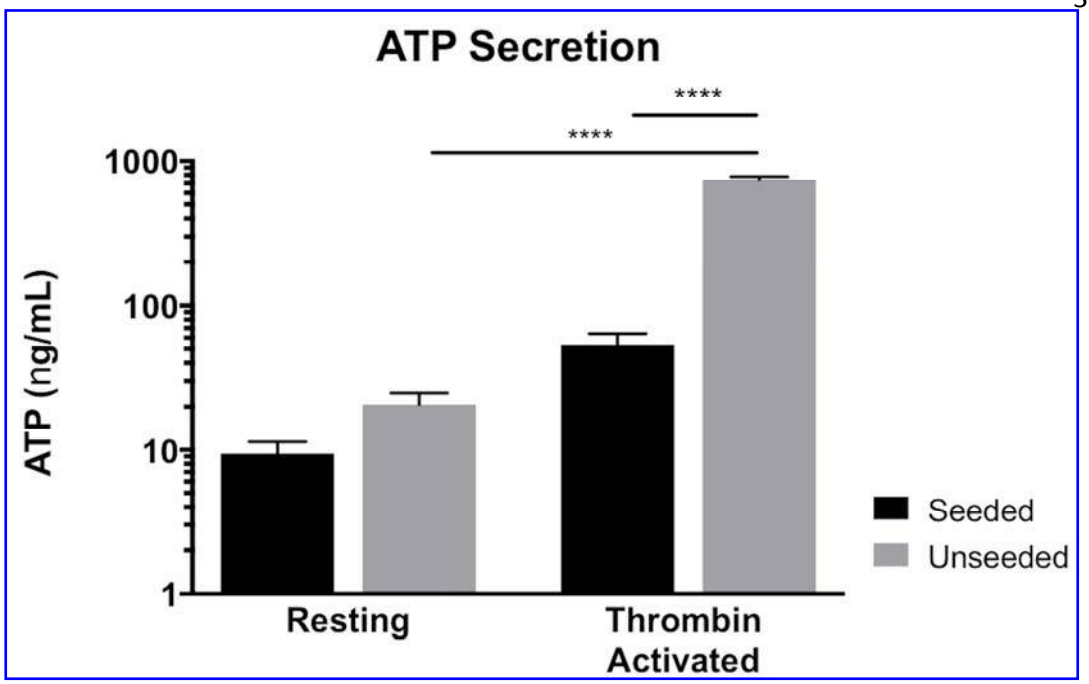

Figure 6. Cell seeding reduced measurable ATP from thrombin-activated platelets. The quantity of ATP derived from thrombin-activated platelets in the presence of BM-MNC seeded scaffolds was significantly less than in the presence of unseeded scaffolds ($^{****}p < 0.001$). In addition, after incubation with unseeded scaffolds, a significant difference in the amount of ATP derived from thrombin-activated and resting platelets was found ($^{****}p < 0.001$), but no difference was observed in the seeded group, suggesting that BM-MNC seeding may regulate platelet function.

Tissue Engineering
Role of Bone Marrow Mononuclear Cell Seeding for Nanofiber Vascular Grafts (DOI: 10.1089/ten.TEA.2017.0044)
This paper has been peer-reviewed and accepted for publication, but has yet to undergo copyediting and proof correction. The final published version may differ from this proof.

Figure Legends

Figure 1. Scaffold characterization. SEM images of luminal (A) and **adventitial** (B) surfaces of the electrospun scaffold. SEM of a BM-MNC-seeded scaffold luminal surface (C). Implantation of a seeded graft **(D)** in the murine **infrarenal** IVC interposition model. Fiber diameter (E) and pore size (F) for luminal surface (Fiber diameter: 0.61 ± 0.27µm, pore size: 9.71 ± 0.16µm). I*n vitro* degradation mechanical values of ultimate tensile strength (UTS) (G), percent elongation to failure (H), and Young's Modulus (I). Scale bar = 50µm.

Figure 2. Lumen diameter over time by serial ultrasound. Serial ultrasound of implanted TEVGs performed at 2, 4, 8, 12, and 24 weeks after graft implantation indicated a significant difference in lumen diameter between the seeded and unseeded groups as early as 4 weeks after implantation that was maintained throughout the 6-month time course (A, $^{****}p < 0.0001$, $^{*}p < 0.05$, $^{**}p < 0.005$). Representative ultrasound images from each time points (B-K, respectively), demonstrating patent grafts characterized by color Doppler flow through the lumen (B, D, F, H, J) in the seeded group and occluded grafts in the unseeded group (C, E, G, I, K). Color Doppler signals in the unseeded group may indicate the presence of collateral vasculature surrounding stenotic TEVGs. **The white dotted lines indicate the luminal and adventitial surfaces of the TEVGs.** Scale bar = 2.0 mm.

Figure 3. Histological assessment of vascular neotissue formation after 6 months. Histomorphometric comparison of the lumen diameter measurements (A) and graft patency (B) between the seeded and unseeded groups demonstrates that BM-MNC seeding prevents occlusion in the nanofiber scaffold ($^{****}p < 0.0001$, $^{***}p = 0.0003$). Histologic comparison between seeded and unseeded scaffolds demonstrated vascular neotissue formation in seeded grafts characterized by mature extracellular matrix (ECM) on the luminal and adventitial graft surfaces, adequate cellular infiltration, and minimal vascular calcification. Representative photomicrographs for each group (Seeded: C, E-H; Unseeded: D, I-L) are shown for H&E (C and D), Masson's trichrome (E and I), Hart's (G and

K), von Kossa (F and J), and Picrosirius red stains (H and L). Scale bar = 200μm for C and D, and 100μm otherwise.

Figure 4. BM-MNC seeding of electrospun TEVG modulated host inflammatory cell infiltration and phenotype. F4/80 staining of seeded (A) and unseeded (B) electrospun TEVGs. Phenotypic characterization of TEVG macrophages demonstrated iNOS$^+$ (Seeded: C; Unseeded: E) and CD206$^+$ (Seeded: D; Unseeded: F) cells. **F4/80$^+$ cells in the seeded vs. unseeded group at 6 months (G); seeded group revealed significantly less macrophage infiltration ($^*p < 0.05$). iNOS$^+$ and CD206$^+$ cells in the seeded vs. unseeded group at 6 months (H); unseeded group showed significantly less CD206$^+$ cells** ($^{****}p < 0.0001$). Scale bar = 20μm.

Figure 5. Cell-seeded nanofiber scaffolds are characterized by well-organized and mature vascular neotissue. Immunofluorescent staining of BM-MNC seeded scaffolds indicated the formation of well-organized neo-intima characterized by a medial α-SMA$^+$ (red) smooth muscle cell layer lined by CD31$^+$ (green) endothelial cells (A, B, arrowheads denote background staining due to remaining scaffold material). SM-MHC staining (red) confirmed that the medial smooth muscle cells in the seeded group were mature and contractile (B, inset). Unseeded TEVG neotissue was characterized by an unorganized population of α-SMA$^+$ and CD-31$^+$ cells (C), with evidence of re-canalization (D, arrowheads indicate neovascularization of stenotic tissue). **Quantification of eNOS and ACTA2 gene transcription by RT-qPCR (E); less ACTA2 and significantly more eNOS gene transcription in the seeded group ($^{**}p < 0.005$).** Scale bar = 50μm for A and C, 10μm for B and D.

Figure 6. Cell seeding reduced measurable ATP from thrombin-activated platelets. The quantity of ATP derived from thrombin-activated platelets in the presence of BM-MNC seeded scaffolds was significantly less than in the presence of unseeded scaffolds ($^{****}p <$ 0.001). In addition, after incubation with unseeded scaffolds, a significant difference in the

amount of ATP derived from thrombin-activated and resting platelets was found ($^{****}p < 0.001$), but no difference was observed in the seeded group, suggesting that BM-MNC seeding may regulate platelet function.

Tissue Engineering
Role of Bone Marrow Mononuclear Cell Seeding for Nanofiber Vascular Grafts (DOI: 10.1089/ten.TEA.2017.0044)
This paper has been peer-reviewed and accepted for publication, but has yet to undergo copyediting and proof correction. The final published version may differ from this proof.